

Holographic pomeron: Saturation and DIS

Alexander Stoffers* and Ismail Zahed†

Department of Physics and Astronomy, Stony Brook University, Stony Brook, New York 11794-3800, USA

(Received 1 October 2012; published 25 April 2013)

We briefly review the approach to dipole-dipole scattering in holographic QCD developed in G. Basar *et al.*, Phys. Rev. D **85**, 105005 (2012), based on a stringy Schwinger mechanism. The pomeron emerges through the exchange of closed strings between the dipoles and yields Regge behavior for the elastic amplitude. We calculate curvature corrections to this amplitude in both a conformal and confining background, identifying the holographic direction with the virtuality of the dipoles. The *wee-dipole* density is related to the string tachyon diffusion in both virtuality and the transverse directions. We give an explicit derivation of the dipole saturation momentum both in the conformal and confining background. Our holographic result for the dipole-dipole cross section and the *wee-dipole* density in the conformal limit are shown to be identical in form to the BFKL pomeron result when the noncritical string transverse dimension is $D_{\perp} = 3$. The total dipole-dipole cross section is compared to DIS data from HERA.

DOI: [10.1103/PhysRevD.87.075023](https://doi.org/10.1103/PhysRevD.87.075023)

PACS numbers: 11.25.Tq, 13.60.Hb, 13.85.Lg

I. INTRODUCTION

In perturbative QCD, dipole-dipole as onium-onium scattering has long been used to describe high energy scattering, [1–13]. In the 1-pomeron exchange, this is equivalent to the BFKL approach [14]. The scattering amplitude can be defined through the convolution of densities of the *wee-dipoles* originating from the parent dipoles and diffusing along the rapidity direction in transverse space. This fundamental diffusion was foreseen long ago by Gribov and will be referred to as Gribov’s diffusion [15].

Holographic QCD offers a nonperturbative framework for discussing diffractive scattering at large number of colors N_c and strong t’Hooft coupling $\lambda = g^2 N_c$. Originally, elastic and inelastic parton-parton and dipole-dipole scattering in the pomeron limit were addressed using noncritical and variational surface exchanges in conformal and nonconformal anti-de Sitter (AdS) backgrounds [16–20]. The pomeron and reggeon emerge from an imaginary contribution to the Nambu-Goto string in confined AdS with an unexplained multibranch structure. Recently, key aspects of the pomeron were shown to follow from a stringy Schwinger mechanism in dipole-dipole scattering with different pomeron parameters [1]. The unexplained multibranch structure observed in Refs. [18–20] follows from the N -ality of the dipole source.

An alternative derivation of the pomeron as a graviton using the Virasoro-Shapiro amplitude in ten dimensions was suggested in Refs. [21–25]. While in flat space the amplitude is real, it was argued that the effect of curvature will cause it to reggeize with the spin-2 graviton transmuting to a spin-2 glueball Regge trajectory timelike and the pomeron spacelike. While the surface exchange and the graviton approaches for the strongly coupled pomeron are similar in spirit, they differ in content. Indeed, in conformal

AdS the multigraviton interactions are dominant for small dipoles [17], while in confined AdS gravitons are massive on distance scales of the order of the confinement scale where the dipole-dipole interaction is dominated by massless string exchange [1]. In the conformal limit, both approaches appear similar although with totally different parameters for the pomeron as the underlying exchange is different.

Diffractive dipole-dipole scattering in holographic QCD is dominated by closed string pair creation at large rapidity χ and impact parameter \mathbf{b}_{\perp} . In Ref. [1] it was argued that the elastic and forward part of the dipole-dipole scattering amplitude is totally dominated by a string pair creation process reminiscent of the Schwinger particle pair creation process whereby the induced longitudinal electric field on the exchanged string world sheet is $E/\sigma_T = \tanh(\chi/2)$. This induced electric field causes the string to feel a longitudinal acceleration and consequently a local Unruh temperature. The latter is an alternate and novel way of physically justifying Gribov’s wee parton diffusion in the context of the pomeron exchange.

In curved AdS, the scattering amplitude in holography is closely related to Gribov diffusion in curved space. As the analysis of the Schwinger mechanism in Ref. [1] was carried using string exchange in Witten’s confining background in the near horizon limit (flat space), it is important to extend it to curved AdS space. Below, we show that the extension to conformal AdS₃ (short for transverse AdS₅) yields a result that is similar to the one for the onium-onium scattering amplitude following from the BFKL pomeron exchange in QCD [2–13], the differences being the pomeron intercept and diffusion constant. We also discuss the concept of dipole saturation for conformal and confining AdS₃, a point of intense interest both at HERA and present and future colliders.

Saturation in the context of holographic models was also discussed recently in Refs. [26,27] using different

*alexander.stoffers@stonybrook.edu

†zahed@tonic.physics.sunysb.edu

arguments. The arguments presented in Refs. [26,27] are based on the Virasoro-Shapiro amplitude in ten dimensions [21,22]. As we noted above this construction is far from the pomeron kinematics in confining geometries with massive glueballs. The saturation analysis in Refs. [28,29] makes use of a Euclidean surface that does not contain the stringy Schwinger mechanism with an essential singularity in the limit of a zero rapidity gap. The surface exchanges in Refs. [1,18–20] do. A more model dependent approach to saturation through the use of a black disk approximation for the dipole-dipole cross section in transverse AdS was recently discussed in Ref. [30].

In Refs. [1,18–20] it was suggested that in the pomeron regime with confining geometry, the string is far from critical and supersymmetric with $D_{\perp} < 8$. Indeed, most of the QCD string simulations spacelike for heavy quarkonia indicate that $D_{\perp} = 2$. Timelike the QCD gluon ladder exchange is conformal at weak coupling [14], so it is natural to enforce conformality on the string exchange. As we will show below, this is naturally achieved by extending the string in the holographic direction in $D_{\perp} = 3$ with hyperbolic or AdS curvature.

The ensuing *wee-dipole* distribution and cross sections at strong coupling compare favorably with those obtained using the BFKL resummation kernel at weak coupling [2–13]. The holographic pomeron in $D_{\perp} = 3$ follows from an effective string theory perhaps of the type advocated by Luscher [31]. While we will use holographic QCD in the form of AdS₅ with a wall as a model throughout, a more systematic approach within holography and following Luscher’s long string arguments may be sought in AdS along the arguments in Ref. [32].

In Sec. II, we briefly review the holographic Schwinger mechanism for dipole-dipole scattering presented in Ref. [1]. The pomeron parameters are distinct from those reported in Refs. [18–20]. In Sec. III, we show that the ensuing dipole-dipole cross section is analogous to the cross section for onium-onium scattering in BFKL-resummed QCD [3]. In Sec. IV, we suggest a holographic correspondence between dipole-dipole scattering of varying sizes and parton-parton scattering of varying scales, whereby the scale is identified with the holographic direction z [21]. In Sec. V, we derive the *wee-dipole* density and define the saturation momentum for dipole-dipole scattering through the total inclusive cross section both for the conformal as well as the confining geometry (conformal plus a hard wall). For the conformal background, our results are compared to the perturbative QCD dipole-dipole scattering result using BFKL methods. We compare our results for the proton structure function F_2 to HERA data in Sec. VI. Our conclusions are in Sec. VII.

This paper contains a number of novel relations and results in comparison to the existing literature addressing the pomeron problem in the context of holography. In Sec. II, we show anew that the dipole-dipole amplitude is

dominated by the tachyon of the closed and noncritical bosonic string, a very important physical point not noted in Ref. [1]. In Sec. III, the dipole-dipole cross section is explicitly constructed and shown to correctly match the onium-onium cross section in QCD for $D_{\perp} = 3$, albeit at strong coupling. In Sec. IV, we show how to construct the *wee-dipole* density in the context of holography that leads to a new definition of the concept of saturation momentum in holography. In Sec. V, we show anew that the holographic saturation momentum in the conformal limit is in one-to-one correspondence with the QCD saturation momentum obtained in the 1-pomeron approximation provided that $D_{\perp} = 3$. In particular, holography suggests that at low Bjorken x , the saturation momentum scales as $1/x\sqrt{D_{\perp}/6\sqrt{\lambda}}$. In Sec. VI, a new and explicit holographic expression for the F_2 -structure function in DIS is derived that is valid both in the conformal and confining regime. In particular, a specific nonperturbative region in the cumulative HERA data is identified using these newly derived saturation momenta.

II. STRINGY SCHWINGER MECHANISM

The eikonalized dipole-dipole scattering amplitude \mathcal{T} in Euclidean space takes the following form [33]:

$$\frac{1}{-2is} \mathcal{T}(\theta, q) \approx \int d\mathbf{b}_{\perp} e^{iq_{\perp} \cdot \mathbf{b}_{\perp}} \mathbf{W} \mathbf{W}, \quad (1)$$

with

$$\mathbf{W} \mathbf{W} = \langle (\mathbf{W}(\theta, \mathbf{b}_{\perp}) - \mathbf{1})(\mathbf{W}(0, 0) - \mathbf{1}) \rangle, \quad (2)$$

and

$$\mathbf{W}(\theta, \mathbf{b}_{\perp}) = \frac{1}{N_c} \text{Tr} \left(\mathbf{P}_c \exp \left(ig \int_{C_{\theta}} d\tau A(x) \cdot v \right) \right) \quad (3)$$

is the normalized Wilson loop for a dipole, $\langle \mathbf{W} \rangle \equiv \mathbf{1}$. In Euclidean geometry C_{θ} is a closed rectangular loop of width a that is slopped at an angle θ with respect to the vertical imaginary time direction. The two-dimensional integral in (1) is over the impact parameter \mathbf{b}_{\perp} with $t = -q_{\perp}^2$, and the averaging is over the gauge configurations using the QCD action.

Following Refs. [16–20,1,21–24], the averaging in (2) will be sought in the context of holography. For small size dipoles, the chief contribution to (2) stems from the exchange of a closed string whose world sheet spans a funnel between the two dipoles as first suggested by Veneziano in the context of the topological expansion [34]. In Ref. [1], (2) was estimated using a (quantum) closed string exchange

$$\mathbf{W} \mathbf{W} = g_s^2 \int_0^{\infty} \frac{dT}{2T} \mathbf{K}(T), \quad (4)$$

with $\mathbf{K}(T)$ a string partition function with cylinder topology of modulus T with twisted boundary conditions.

The string coupling $g_s \sim 1/N_c$ reflects on the subleading (handle contribution) character of the exchange in large N_c .

The dominant contribution to (4) was found to follow from the poles of the longitudinal stringy mode contributions in Ref. [1],

$$\mathbf{W}\mathbf{W}_{\text{poles}} \approx \frac{g_s^2}{4} \sum_{k=1}^{\infty} \frac{(-1)^k}{k} \left(\frac{k\pi}{\chi}\right)^{D_{\perp}/2} \times \frac{aa'}{\alpha'} e^{-k\mathbf{b}_{\perp}^2/2\chi\alpha' + D_{\perp}\chi/12k}, \quad (5)$$

with $\alpha' = 1/(2\pi\sigma_T)$. The summation over k is over the N -ality of the Wilson loop. $k = 1$ for a loop in the fundamental representation. This will be understood below. At large χ the string freezes in its ground state. (5) can be rewritten as

$$\mathbf{W}\mathbf{W}_{\text{poles}} \approx \frac{g_s^2}{4} \left(\frac{\pi}{\sigma_T}\right)^{D_{\perp}/2} \sum_{k=1}^{\infty} \frac{(-1)^k}{k} \frac{aa'}{\alpha'} \mathbf{K}_k(\chi, \mathbf{b}_{\perp}). \quad (6)$$

The emerging propagator at the poles,

$$\mathbf{K}_k(\chi, \mathbf{b}_{\perp}) = \left(\frac{k}{2\pi\alpha'\chi}\right)^{D_{\perp}/2} e^{-k\mathbf{b}_{\perp}^2/2\chi\alpha' + D_{\perp}\chi/12k}, \quad (7)$$

satisfies a diffusion equation in flat space,

$$\left(\partial_{\chi} - \frac{D_{\perp}}{12k}\right) \mathbf{K}_k(\chi, \mathbf{b}_{\perp}) = \mathbf{D}_k \nabla_{\perp}^2 \mathbf{K}_k(\chi, \mathbf{b}_{\perp}), \quad (8)$$

with a diffusion constant in rapidity space $\mathbf{D}_k = \alpha'/2k$. For long strings with \mathbf{b}_{\perp} large, the pertinent AdS metric on the string is nearly flat. The effects of curvature will become apparent at intermediate \mathbf{b}_{\perp} and will be addressed below.

For long strings, the diffusion propagator (7) emerges as the natural version of the periodic string propagator in (4) in the diffusive regime $\mathbf{b}_{\perp} \sim \sqrt{\chi\alpha'}$. We note that (8) is just the proper time evolution of the tachyonic string mode,

$$(\partial_{T_{\perp}} + (M_0^2 - \nabla_{\perp}^2)) \mathbf{K}_k(T_{\perp}, M, \mathbf{b}_{\perp}) = 0, \quad (9)$$

after the identification $T_{\perp} = \mathbf{D}_k\chi$. The tachyonic mass follows from the harmonic string spectrum:

$$M_n^2 = \frac{4}{\alpha'} \left(n - \frac{D_{\perp}}{24}\right) \rightarrow -\frac{D_{\perp}}{6\alpha'}. \quad (10)$$

The occurrence of (9) is naturally explained by noting that the dominant contribution to the closed string propagator in (4) stems from short proper times $T = 2\pi k/\chi < 1$ [1]. We recall that T is the period of the open string exchange by T -duality. So $T = 1/(\mathbf{b}_{\perp}T_U)$ plays effectively the role of a ‘‘temperature’’ for the open string. Indeed explicit arguments in Ref. [1] show that $T_U \approx \chi/2\pi\mathbf{b}_{\perp} > 1$ acts as an Unruh temperature on the open string world sheet after properly identifying the induced longitudinal electric field at the origin of this phenomenon. Much like the heavy-quark string dimensionally reduces and diffuses at finite and real temperature [35], so does the

holographic string under the effect of T_U . This analogy provides a physically novel interpretation of Gribov’s wee parton diffusion in the context of the pomeron exchange [15]. Since the Unruh temperature is lower than the Hagedorn temperature for long and noncritical strings, the dominant string mode is the tachyon.

III. ONIUM-ONIUM SCATTERING

QCD dipole-dipole scattering at large χ and weak coupling has been extensively discussed by Mueller and others [2,3,3–12]. This approach to high-energy hadron-hadron scattering was pioneered by Gribov [15]. Typically, the scattering is viewed as a parent dipole of size a depleting into a cascade of daughter dipoles (*wee-dipoles*) and smashing against a similar parent dipole of size a' for fixed income parameter \mathbf{b}_{\perp} . The onium-onium cross section in the single BFKL exchange reads [3]

$$\sigma_{\text{tot}}^{\text{BKFL}}(\chi) = 2\pi \frac{\lambda^{3/2}}{N_c^2} aa' \frac{e^{(\alpha_{\text{BKFL}}-1)\chi}}{(4\pi\mathbf{D}^{\text{BKFL}}\chi)^{1/2}}, \quad (11)$$

with

$$\alpha^{\text{BKFL}} = 1 + \frac{\lambda}{\pi^2} \ln 2, \quad \mathbf{D}^{\text{BKFL}} = 7\lambda\zeta(3)/(8\pi^2) \quad (12)$$

the BFKL intercept and diffusion constant, respectively. ζ is the Riemann zeta function.

The holographic dipole-dipole scattering amplitude in a confining (Witten) AdS background in the single funnel-exchange approximation was worked out in Ref. [1] in the near horizon limit or, equivalently, for long strings. In this work, the confining background will be simplified to AdS with a wall. The dipole-dipole cross section for a single string exchange in the near horizon limit is [1]

$$\sigma_{\text{tot}}(\chi) = \frac{g_s^2}{2\alpha'} (2\pi^2\alpha')^{D_{\perp}/2} aa' \frac{e^{(\alpha_{\text{P}}-1)\chi}}{(4\pi\mathbf{D}\chi)^{D_{\perp}/2-1}}. \quad (13)$$

In leading order in $1/\sqrt{\lambda}$,

$$\alpha_{\text{P}} = 1 + \frac{D_{\perp}}{12}, \quad \mathbf{D} = \frac{\alpha'}{2} = \frac{1}{2\sqrt{\lambda}} \quad (14)$$

are the holographic intercept and diffusion constant, respectively. For AdS with a wall, the *effective* string tension will be defined as

$$g_s \equiv \kappa \frac{1}{4\pi\alpha'^2 N_c} \equiv \kappa \frac{\lambda}{4\pi N_c}, \quad (15)$$

with $\alpha' = 1/\sqrt{\lambda}$ the string tension (in units of the AdS radius). We note that the $1/N_c$ dependence of the string coupling does not depend on the nature of the holographic model, but the λ dependence does. The parameter κ follows from the unfixed overall constant in the derivation of the dipole-dipole amplitude, see Eq. (32) in Ref. [1], where it was absorbed in the definition of the dipole size. Here we have chosen to absorb it into the definition of the string

coupling instead, hence the label *effective*. Below, it will be fixed phenomenologically to $\kappa = 2.5$.

A comparison of (14) to (11) suggests that effectively $D_{\perp} = 3$, an observation that will be iterated below. In a way, the results of Ref. [1] can be thought as following from a noncritical string theory in $D_{\perp} + 2$ dimensions, as perhaps advocated by Luscher a while ago [31]. In this effective string theory, the Polyakov action is the leading and universal contribution for long strings.

The dependence on aa' in (11) and (13) is noteworthy as it differs from $a^2a'^2$ in perturbation theory. In the string description this follows readily from the fact that the string attachment to the dipole only depends on a and a' at each end respectively. This is not the case for 2 gluon exchange in perturbation theory where each gluon attaches to a and a' respectively, thus a^2 and a'^2 . In both cases the dipole-dipole cross section vanishes as $a, a' \rightarrow 0$ as it should.

IV. CURVED TACHYON DIFFUSION

The preceding observations hold true even in curved space whereby the string in a curved background is also subjected to a high Unruh temperature at the end points. Although the exact form of the string propagator in curved space in (4) is unknown, we expect the longitudinal pole structure leading to the reduction (5) to remain unchanged since it follows from short proper times, i.e., $T \sim 1/\chi < 1$, which are insensitive to curvature. Since $\chi > 1$ we still expect a large Unruh temperature on the dual open string exchange, and therefore a reduction of the tachyonic string to transverse space, which is curved on the diffusion time scale. Tachyon diffusion in curved space follows through

$$\left(\partial_{T_{\perp}} + \left(M_0^2 - \frac{1}{\sqrt{g_{\perp}}} \partial_{\mu} g_{\perp}^{\mu\nu} \sqrt{g_{\perp}} \partial_{\nu}\right)\right) \Delta_{\perp}(x_{\perp}, x'_{\perp}) = 0, \quad (16)$$

where we have suppressed \mathbf{b}_{\perp} , M to alleviate the notation. The metric g_{\perp} in (16) is that of the transverse space with positive signature. (16) is the curved space generalization of (9). Below, we show how the curved diffusion propagator Δ_{\perp} can be substituted to \mathbf{K}_k to generalize (5)–(7) to curved AdS. In general x_{\perp} is an arbitrary point in D_{\perp} . In hyperbolic AdS type spaces it is useful to separate $x_{\perp} = (\mathbf{x}, z)$ with z along the holographic direction and \mathbf{x} in the two-dimensional physical space for $D_{\perp} = 3$ for instance with diffusion in AdS₃. The formal solution to (16) reads

$$\Delta_{\perp}(x_{\perp}, x'_{\perp}) = \langle x_{\perp} | e^{-T_{\perp}(M_0^2 - \nabla_C^2)} | x'_{\perp} \rangle, \quad (17)$$

with ∇_C^2 the curved Laplacian in (16) and $T_{\perp} = \mathbf{D}\chi \gg 1$ for $k = 1$. The transverse evolution propagator Δ_{\perp} in (17) ties to the tachyon propagator $\mathbf{G}(j)$,

$$\langle x_{\perp} | \mathbf{G}(j) \equiv (j + (M_0^2 - \nabla_C^2))^{-1} | x'_{\perp} \rangle, \quad (18)$$

through an inverse Mellin transform

$$\Delta_{\perp} = \int_C \frac{dj}{2i\pi} e^{jT_{\perp}} \mathbf{G}(j), \quad (19)$$

with C a pertinent contour in the complex j plane at the rightmost of all singularities. The tachyon propagator in (18) obeys the curved equation

$$(j + (M_0^2 - \nabla_C^2)) \mathbf{G}(j, x_{\perp}, x'_{\perp}) = \frac{1}{\sqrt{g}} \delta_{D_{\perp}}(x_{\perp} - x'_{\perp}). \quad (20)$$

A similar propagator was noted in Ref. [23] starting from the graviton using the critical closed string scattering amplitude in ten dimensions.

A. Conformal

In transverse hyperbolic space AdS _{D_{\perp}} with metric

$$ds_{\perp}^2 = \frac{1}{z^2} (d\mathbf{b}_{\perp}^2 + dz^2), \quad (21)$$

all length scales are measured in units of the AdS radius which is set to 1, and reinstated at the end by inspection. The propagator for a scalar field is given by [36,37]

$$\mathbf{G}_{D_{\perp} \text{ odd}}(j, \xi) = \frac{1}{4\pi} \left(\frac{-1}{2\pi \sinh(\xi) \frac{d}{d\xi}} \right)^{m-1} \frac{e^{-v\xi}}{\sinh(\xi)} \quad (22)$$

for $D_{\perp} = 2m + 1$ and

$$\mathbf{G}_{D_{\perp} \text{ even}}(j, \xi) = \frac{1}{2\pi} \left(\frac{-1}{2\pi \sinh(\xi) \frac{d}{d\xi}} \right)^m \mathcal{Q}_{\nu-1/2}(\cosh(\xi)) \quad (23)$$

for $D_{\perp} = 2m$ with

$$\nu^2 = j - j_0, \quad j_0 = -M_0^2 - (D_{\perp} - 1)^2/4. \quad (24)$$

\mathcal{Q} is a Legendre function of the second kind. The chordal distance ξ is defined through

$$\cosh \xi = 1 + d = 1 + \frac{\mathbf{b}_{\perp}^2 + (z - z')^2}{2zz'}, \quad (25)$$

which gives for $\frac{\mathbf{b}_{\perp}^2}{2zz'} \gg 1$

$$\xi \sim \ln\left(\frac{\mathbf{b}_{\perp}^2}{zz'}\right), \quad \sinh(\xi) \sim \frac{\mathbf{b}_{\perp}^2}{2zz'}. \quad (26)$$

For $D_{\perp} = 3$, inserting the conformal propagator (22) in (19) yields the conformal evolution kernel,

$$\Delta_{\perp}(\chi, \xi) = \frac{e^{j_0 \mathbf{D}\chi}}{(4\pi \mathbf{D}\chi)^{3/2}} \frac{\xi e^{-\frac{\xi^2}{4\mathbf{D}\chi}}}{\sinh(\xi)}, \quad (27)$$

with the diffusion constant $\mathbf{D} = \alpha'/2 = 1/(2\sqrt{\lambda})$ for conformal AdS₃, after restricting the N -ality to $k = 1$. This heat kernel was obtained in Ref. [38] using a group theoretical approach. (27) shows that in conformal AdS₃, the tachyon mode of the bosonic string diffuses in hyperbolic space along the geodesic distance as measured by ξ which is about twice the chordal distance for small displacement, i.e., $\xi^2 \approx 2d \ll 1$. Again the rapidity χ plays the role of time.

B. Confining

Confinement in AdS is captured in a simplified way by the hard-wall model, whereby only a slice of the AdS space is considered with $0 \leq z \leq z_0$ and $z_0 \approx 1/\Lambda$ setting up the confinement scale [22]. In this case, all scales are set by z_0 implicitly in the intermediate expressions and explicitly in the final ones. We note that in the hard wall model we still use the identification $\alpha' \equiv l_s^2/z_0^2 \equiv \sqrt{\lambda}$.

To simplify the analysis for the curved diffusion, we define the total *wee-dipole* density $\mathbf{N} = \Delta/(zz')^{D_\perp-2}$. Since the scattering amplitude is symmetric under the interchange of the two dipoles and we are going to identify z, z' with the effective size of the dipoles, the correct rescaling of \mathbf{N} is by powers of zz' . Using the conformal variable $u = -\ln(z/z_0)$, the diffusion equation for the dipole density reads

$$(\partial_{T_\perp} + (M_0^2 + D_\perp - 2) - \partial_u^2 - e^{2u}\nabla_{\mathbf{b}_\perp}^2)\mathbf{N} = 0. \quad (28)$$

The proper time evolution of \mathbf{N} in AdS amounts to a transport or diffusion equation, with the initial condition

$$\mathbf{N}(T_\perp = 0, u, u', \mathbf{b}_\perp) = \delta(u - u')\delta(\mathbf{b}_\perp) \quad (29)$$

as one-dipole per unit area in the transverse \mathbf{b}_\perp .

The boundary condition for solving (28) follows from the conservation of the diffusion charge in the slab $0 \leq z \leq z_0$ or $0 \leq u \leq \infty$,

$$\begin{aligned} \frac{d}{dT_\perp} \int dud\mathbf{b}_\perp e^{T_\perp(M_0^2 + D_\perp - 2)}\mathbf{N} \\ = \int d\mathbf{b}_\perp e^{T_\perp(M_0^2 + D_\perp - 2)}\partial_{u=0}\mathbf{N}, \end{aligned} \quad (30)$$

assuming that the diffusion current vanishes at $\mathbf{b}_\perp = \infty$ and at $u = \infty$ (UV boundary) as no holographic source is subsumed. Thus, the Neumann boundary condition

$$\partial_{u=0}\mathbf{N} = 0 \quad (31)$$

enforces that the (singlet) *wee-dipole* current does not leak in the infrared at $z = z_0$. As a result,

$$\int dud\mathbf{b}_\perp e^{T_\perp(M_0^2 + D_\perp - 2)}\mathbf{N} \equiv 1 \quad (32)$$

is fixed both in the conformal and confining case. Other boundary conditions on the wall, e.g., absorptive or mixed, will result in *wee-dipole* current loss in the infrared or confining region, with (32) less than 1. While intricate physically, these boundary conditions will be pursued elsewhere.

The solution to (28) subject to (29)–(31) is readily obtained by the image method for the current conserving Neumann boundary condition

$$\begin{aligned} \mathbf{N}(T_\perp, u, u', \mathbf{b}_\perp) &= \frac{1}{z_0^2} e^{u'+u} \Delta(\chi, \xi) + \frac{1}{z_0^2} e^{u'-u} \Delta(\chi, \xi_*) \\ &= \frac{1}{zz'} \Delta(\chi, \xi) + \frac{z}{z'z_0^2} \Delta(\chi, \xi_*), \end{aligned} \quad (33)$$

with the conformal solution (27) for $\Delta(\chi, \xi)$. The invariance of the interchange of the two dipoles in the conformal case gets affected in the confining contribution [second part in (33)]. The chordal distances follow from (25) as

$$\begin{aligned} \cosh \xi &= \cosh(u' - u) + \frac{1}{2} \mathbf{b}_\perp^2 e^{u'+u}, \\ \cosh \xi_* &= \cosh(u' + u) + \frac{1}{2} \mathbf{b}_\perp^2 e^{u'-u}, \end{aligned} \quad (34)$$

with $-u$ the image of u with respect to the holographic wall at $u = 0$.

C. Wee-dipole density

\mathbf{N} obeys a ‘‘Markovian’’-type chain rule,

$$\begin{aligned} \int du'' d\mathbf{b}_\perp'' \mathbf{N}(T_\perp - T_\perp'', u, u'', \mathbf{b}_\perp - \mathbf{b}_\perp'') \\ \times \mathbf{N}(T_\perp'' - T_\perp', u'', u', \mathbf{b}_\perp'' - \mathbf{b}_\perp') \\ = \mathbf{N}(T_\perp - T_\perp', u, u', \mathbf{b}_\perp - \mathbf{b}_\perp'), \end{aligned} \quad (35)$$

which follows readily from the diffusion evolution kernel as a propagator in rapidity space. (35) suggests a ‘‘Weizsaecker-Williams’’ analogy for the virtual dipole field surrounding each of the initial projectile and target dipole. Thus, the total number of *wee-dipoles* either in the target or the projectile follows from the normalization

$$N_{wee} = \int dud\mathbf{b}_\perp \mathbf{N} = e^{-T(M_0^2 + D_\perp - 2)} \equiv (s/s_0)^{\alpha_P - 1} \quad (36)$$

with the $1/\sqrt{\lambda}$ corrected intercept

$$\alpha_P = 1 + \frac{D_\perp}{12} - \frac{(D_\perp - 1)^2}{8\sqrt{\lambda}}. \quad (37)$$

\mathbf{N} is interpreted as the density of *wee-dipoles* of scale u at a transverse distance \mathbf{b}_\perp sourced by a dipole of scale u' located at $\mathbf{b}'_\perp = \mathbf{0}$. Their total number or multiplicity is given by (36) and grows exponentially with the rapidity $\chi = T/D \equiv \ln(s/s_0)$. This growth is at the origin of the violation of unitarity in the scattering amplitude. Here it is tamed by the eikonized amplitude whereby a class of $1/N_c$ corrections are resummed.

Using the chain rule (35) and the dipole density (33), we obtain the asymptotic dipole density

$$\begin{aligned} \mathbf{N}(\chi, z, z', \mathbf{b}_\perp) &\approx 2 \frac{e^{(\alpha_P - 1)\chi}}{(4\pi\mathbf{D}\chi)^{3/2}} \frac{z}{z'\mathbf{b}_\perp^2} \\ &\times \ln\left(\frac{\mathbf{b}_\perp^2}{zz'}\right) e^{-\ln^2\left(\frac{\mathbf{b}_\perp^2}{zz'}\right)/(4\mathbf{D}\chi)} \end{aligned} \quad (38)$$

in the conformal case and in the limit $\frac{b_{\perp}^2}{2zz'} \gg 1$. The analogue of (38) in the context of onium-onium scattering was discussed in Refs. [3–5]. In particular, in the BFKL 1-pomeron approximation it is given by [3]

$$\mathbf{N}^{\text{BFKL}}(\chi, z, z', \mathbf{b}_{\perp}) \approx 2 \frac{e^{(\alpha^{\text{BFKL}} - 1)\chi}}{(4\pi \mathbf{D}^{\text{BFKL}} \chi)^{3/2}} \frac{z}{z' b_{\perp}^2} \times \ln\left(\frac{b_{\perp}^2}{zz'}\right) e^{-\ln^2\left(\frac{b_{\perp}^2}{zz'}\right) / (4\mathbf{D}^{\text{BFKL}} \chi)}, \quad (39)$$

with the BFKL intercept α^{BFKL} and diffusion constant \mathbf{D}^{BFKL} , see (12). Modulo the pomeron intercept and the diffusion constant, which are different (weak coupling or BFKL versus strong coupling or holography), the holographic result in the conformal limit is identical to the BFKL 1-pomeron approximation. Again, the occurrence of the 3/2 exponent reflects on diffusion in $D_{\perp} = 3$ as noted earlier. It is remarkable that the BFKL resummation of perturbative QCD diagrams is encoded in the stringy Schwinger mechanism discussed in Ref. [1], albeit in hyperbolic space.

Figure 1 shows the distribution of the holographic *wee-dipole* density (33) in solid line versus \mathbf{b}_{\perp} for $z = z' = 1.8 \text{ GeV}^{-1}$ and $\chi = 10$. The dashed curve is the asymptotic distribution (38). Figure 2 shows the distribution of the BFKL *wee-dipole* density (39) (solid line) versus $\mathbf{b}_{\perp}/\sqrt{zz'}$ for also $z = z' = 1.8 \text{ GeV}^{-1}$ and $\chi = 10$. The dashed curve is the improved BFKL result in Ref. [10]. The latter follows from (39) by inserting a factor of 16 in the argument of the logarithm which corresponds to rescaling down the BFKL distribution by a factor of 4 along the $\mathbf{b}_{\perp}/\sqrt{zz'}$ axis. The holographic results use $\mathbf{D} = 0.10$ and $\alpha_{\mathbf{P}} - 1 = 0.146$, while the BFKL results use $\mathbf{D}^{\text{BFKL}} = 0.72$ and $\alpha_{\mathbf{P}} - 1 = 0.477$ with $\lambda = 23$. Both the holographic and the improved distributions are less skewed and more centered. The holographic distribution is less spread than the improved BFKL distribution in \mathbf{b}_{\perp} , therefore less infrared sensitive.

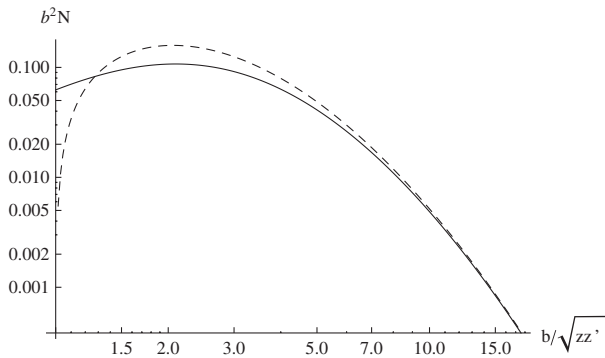


FIG. 1. Holographic *wee-dipole* spatial distributions for $z = z' = 1.8 \text{ GeV}^{-1}$ and $\chi = 10$. Confining density in (33): solid curve; asymptotic density in (38): dashed curve. See text.

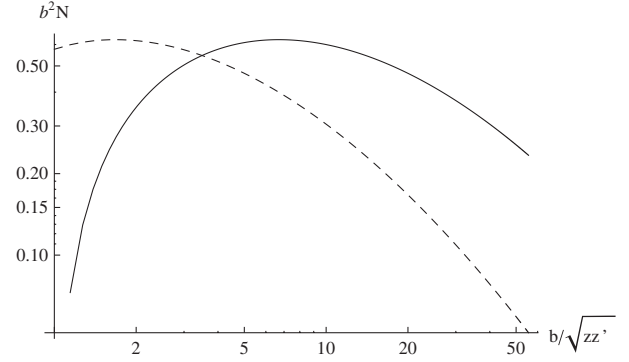


FIG. 2. BFKL *wee-dipole* spatial distributions for $z = z' = 1.8 \text{ GeV}^{-1}$ and $\chi = 10$. BFKL density (39): solid curve; improved BFKL density: dashed curve. See text.

V. SATURATION IN CURVED SPACE

In curved space the holographic picture suggests the identification of the holographic direction with the effective size of the scatterer [21,22,39,40]. We now suggest that dipole-dipole scattering in holography can be thought of as scattering a *wee-dipole* cloud of virtuality $1/z$ onto a *wee-dipole* cloud of virtuality $1/z'$. This leads to the concept of dipole saturation as first discussed in Ref. [41].

For $D_{\perp} = 3$, we identify

$$\frac{aa'}{\alpha'} \mathbf{K}_k(\chi, \mathbf{b}_{\perp}) \rightarrow zz' \mathbf{N}(\chi, z, z', \mathbf{b}_{\perp}). \quad (40)$$

In terms of (40), the leading ($k = 1$) contribution to (5) in a curved AdS background reads

$$\mathbf{W}\mathbf{W}_{\text{poles}} \approx -\frac{g_s^2}{4} (2\pi\alpha')^{3/2} zz' \mathbf{N}(\chi, z, z', \mathbf{b}_{\perp}). \quad (41)$$

The differential dipole-dipole cross section at finite impact parameter is then [1]

$$\frac{d^4 \sigma_{\text{tot}}}{dudu' d\mathbf{b}_{\perp}} = 2(1 - e^{\mathbf{W}\mathbf{W}_{\text{poles}}}). \quad (42)$$

Assuming that the target is a proton with a dipole wave function peaked at some virtuality corresponding to $u_{\mathbf{T}}$, i.e., $\varphi_{\mathbf{T}}(u') = \delta(u' - u_{\mathbf{T}})$, (42) averaged over a target wave function reads

$$\frac{d^3 \sigma_{\text{tot}}}{dud\mathbf{b}_{\perp}} \approx 2(1 - e^{\langle \mathbf{W}\mathbf{W}_{\text{poles}} \rangle}), \quad (43)$$

with only the first cumulant retained and

$$\langle \mathbf{W}\mathbf{W}_{\text{poles}} \rangle = \int dz \varphi_{\mathbf{T}}(z) \mathbf{W}\mathbf{W}_{\text{poles}}. \quad (44)$$

Higher cumulants are suppressed by higher powers of $g_s^2 \approx 1/N_c^2$. This amounts to $z' \rightarrow z_{\mathbf{T}}$ in (41).

(43) suggests the definition of the saturation momentum \mathbf{Q}_s from

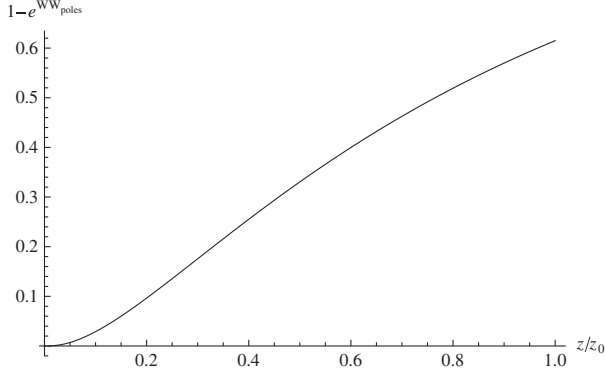


FIG. 3. Saturating behavior of the dipole-dipole cross section (43), at $\chi = 15$ for fixed $\mathbf{b}_\perp = 2 \text{ GeV}^{-1}$. See text.

$$\frac{d^3 \sigma_{\text{tot}}}{du_s d\mathbf{b}_\perp} \equiv 2(1 - e^{-z_s \mathbf{Q}_s / (2\sqrt{2})}), \quad (45)$$

with $\mathbf{Q}_s \equiv -2\sqrt{2}(\mathbf{W}\mathbf{W}_{\text{poles}})/z_s$ fixed by the saturating dipole size $z_s = \sqrt{2}/\mathbf{Q}_s$. This saturating behavior is illustrated in Fig. 3. This is the canonical choice for which

$$(1 - e^{-z_s \mathbf{Q}_s / (2\sqrt{2})}) \rightarrow (1 - e^{-1/2}) \approx 0.4, \quad (46)$$

leading to a scattering amplitude of order 1. The saturation momentum follows from the transcendental equation,

$$\frac{z_s}{\sqrt{2}} \mathbf{Q}_s(\chi, \mathbf{b}_\perp) = \frac{g_s^2}{2} (2\pi\alpha')^{3/2} z_s z_T \mathbf{N}(\chi, z_s, z_T, \mathbf{b}_\perp) = 1. \quad (47)$$

Saturation takes place whenever the dipole density $\mathbf{N} \sim N_c^2/\lambda^{\frac{5}{4}} > 1$ in (hard wall) holography. This is comparable to perturbative QCD with $\mathbf{N} \sim N_c^2/\lambda > 1$. As the dipole density $\mathbf{N}(\chi, z_s, z_T, \mathbf{b}_\perp)$ is peaked around some finite z_s for fixed $\chi, z_T, \mathbf{b}_\perp$, the solution to (47) has in general two solutions. To explicit them, we now need to detail the holographic parameters.

Our set of dimensionless holographic parameters consists of $D_\perp = 3, N_c = 3, \lambda = 23$, and $\kappa = 2.5$. The choice of λ is fixed by the F_2 slope in comparison to the DIS data (see below). The value of κ is fixed by the saturation scale (see below). Since $\lambda = g^2 N_c$, the Yang-Mills coupling is $g^2/4\pi = 0.6$, which is on the strong coupling side.

We note that although the *original* string coupling is small, i.e., $\lambda/4\pi N_c = 0.6 < 1$ as required by holography, the physical value of $N_c < \lambda$ is at odds with the holographic and strong coupling limit. This notwithstanding, our corrected soft pomeron intercept is

$$\alpha_P - 1 = \frac{1}{4} - \frac{1}{2\sqrt{\lambda}} = 0.146. \quad (48)$$

Although this numerical value is on the higher side of the pp scattering data of 0.08, it only refers to the *bare* soft pomeron intercept which is likely to decrease through multipomeron resummation and shadowing.

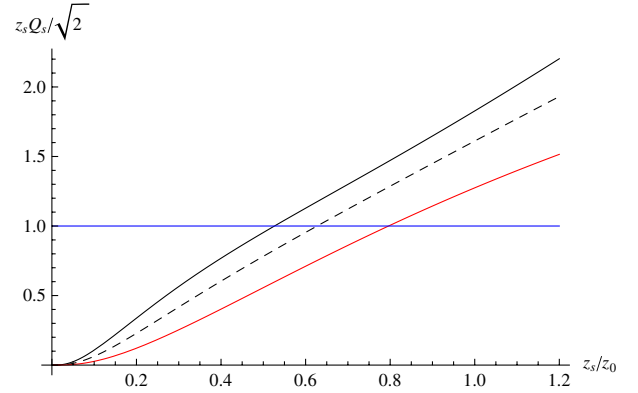


FIG. 4 (color online). Illustration of the solutions to (47) with $\mathbf{b}_\perp^2 = 0 \text{ GeV}^{-2}$ (black, solid), $\mathbf{b}_\perp^2 = 1 \text{ GeV}^{-2}$ (black, dashed) and $\mathbf{b}_\perp^2 = 3 \text{ GeV}^{-2}$ (red) at $\chi = 8$. See text.

Our set of dimensionfull holographic parameters consists of $z_0 = 2 \text{ GeV}^{-1}, z_T = 1.8 \text{ GeV}^{-1}, s_0 = 10^{-1} \text{ GeV}^2$, which are set close to the confining scale in QCD. We kinematically translate the rapidity through

$$\chi = \ln\left(\frac{s}{s_0}\right) \equiv \ln\left(\frac{Q^2}{s_0} \left(\frac{1}{x} - 1\right)\right)$$

using the DIS kinematics (see below). For fixed $\chi = 5$ and $z_T = 2$ and varying \mathbf{b}_\perp , an illustration of (47) is shown in Fig. 4, using these parameters. The numerical dependence of the slope in Fig. 4 near the origin (small z_s/z_0) is linear.

A. Conformal

In the conformal limit, the dipole density is explicit, giving the implicit saturation density,

$$\mathbf{Q}_s(\chi, \mathbf{b}_\perp) = \frac{g_s^2}{\sqrt{2}} (2\pi\alpha')^{3/2} \frac{1}{z_s} \frac{e^{(\alpha_P - 1)\chi}}{(4\pi\mathbf{D}\chi)^{3/2}} \frac{\xi e^{-\frac{\xi^2}{4\mathbf{D}\chi}}}{\sinh(\xi)}. \quad (49)$$

For large transverse separation $\frac{\mathbf{b}_\perp^2}{2z_s z_T} \gg 1$, (49) defines a dipole density in the transverse coordinate,

$$\begin{aligned} \mathbf{Q}_s(\chi, \mathbf{b}_\perp) &\approx \sqrt{2} g_s^2 (2\pi\alpha')^{3/2} \frac{e^{(\alpha_P - 1)\chi}}{(4\pi\mathbf{D}\chi)^{3/2}} \frac{z_T}{\mathbf{b}_\perp^2} \\ &\times \ln\left(\frac{\mathbf{b}_\perp^2}{z_s z_T}\right) e^{-\ln^2\left(\frac{\mathbf{b}_\perp^2}{z_s z_T}\right)/(4\mathbf{D}\chi)}. \end{aligned} \quad (50)$$

The large $\chi = \ln(s/s_0) > 1$ exponential asymptotics of (49) and (50) have two solutions, say $z_{s1} < z_{s2}$. Only the small dipole solution z_{s1} is retained in the conformal case, as the large dipole solution z_{s2} is deep in the infrared and unphysical. In the confined case, it is naturally cut off by the wall (see below). With this in mind and to leading exponential accuracy,

$$\mathbf{Q}_s(\chi, \mathbf{b}_\perp) \approx \frac{z_T}{\mathbf{b}_\perp^2} e^{2\mathbf{D}\chi(\sqrt{1+(\alpha_P - 1)/\mathbf{D}} - 1)}. \quad (51)$$

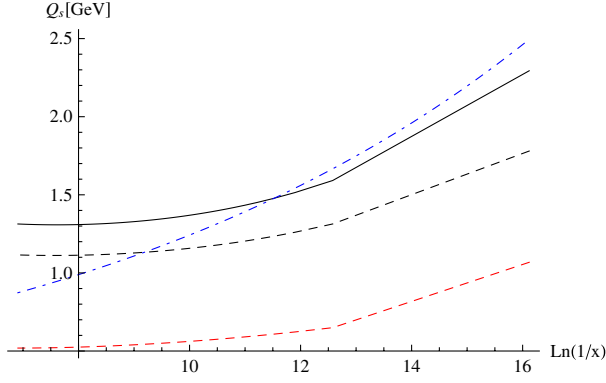


FIG. 5 (color online). x dependence of the saturation momentum (55). Black, solid: $\mathbf{b}_\perp^2 = 0 \text{ GeV}^{-2}$. Black, dashed: $\mathbf{b}_\perp^2 = 1 \text{ GeV}^{-2}$. Dashed red curve: saturation momentum in the conformal limit (49), with $\mathbf{b}_\perp^2 = 1 \text{ GeV}^{-2}$. The dashed dotted blue curve is the GBW saturation momentum from (54). See text.

At large $\sqrt{\lambda}$,

$$\mathbf{Q}_s(\chi, \mathbf{b}_\perp) \approx \frac{z_T}{\mathbf{b}_\perp^2} \left(\frac{1}{x}\right)^{\sqrt{D_\perp/6\sqrt{\lambda}}}, \quad (52)$$

illustrating the smallness of the exponent. For the parameters used above, (51) reads

$$\mathbf{Q}_s(\chi, \mathbf{b}_\perp) \approx \frac{z_T}{\mathbf{b}_\perp^2} \left(\frac{1}{x}\right)^{0.228/2}. \quad (53)$$

An early phenomenological approach to describe DIS data at HERA by Golec-Biernat and Wuesthoff (GBW) in Ref. [13], defines the saturation momentum as

$$Q_s^{\text{GBW}}(x) = \left(\frac{x_0}{x}\right)^{\Lambda/2} \text{ GeV}. \quad (54)$$

HERA data are fitted with $x_0 = 3.04 \cdot 10^{-4}$ and $\Lambda = 0.288$. Note that the GBW saturation momentum corresponds to the substitution $z_s \mathbf{Q}_s / (2\sqrt{2}) \rightarrow (z_s Q_s^{\text{GBW}} / 2)^2$ in (45). While the magnitude of the saturation momentum in our holographic approach can be adjusted by tuning κ , we find that the x dependence of the saturation momentum (53) agrees well with the phenomenological fit in (54) as shown in Fig. 5.

B. Confining

The identification (40) carries over to the confining case. The saturation momentum follows from the transcendental equation

$$\mathbf{Q}_s(\chi, \mathbf{b}_\perp) = \frac{g_s^2}{2} (2\pi\alpha')^{3/2} \frac{e^{(\alpha_P-1)\chi}}{(4\pi\mathbf{D}\chi)^{3/2}} \times \left(\frac{1}{z_s} \frac{\xi e^{-\frac{\xi^2}{4\mathbf{D}\chi}}}{\sinh(\xi)} + \frac{z_s}{z_0^2} \frac{\xi_* e^{-\frac{\xi_*^2}{4\mathbf{D}\chi}}}{\sinh(\xi_*)} \right). \quad (55)$$

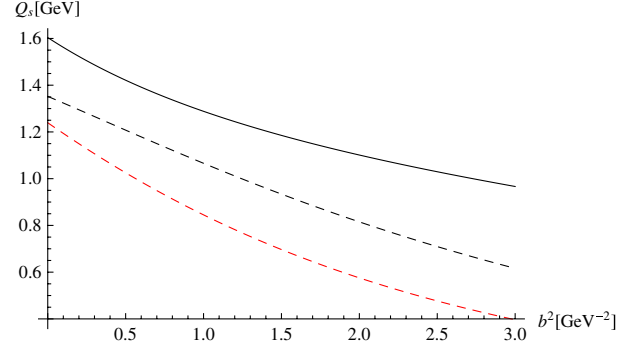


FIG. 6 (color online). Impact parameter dependence of the saturation momentum (55). Upper curve (black, solid): $\chi = 5$; lower curve (dashed, solid): $\chi = 8$. Lowest curve (red, dashed): Saturation momentum in the conformal limit (49), $\chi = 8$. See text.

The x dependence of the saturation momentum [(49) and (55)] is shown in Fig. 5. Figure 6 shows the relevant solution ($z_s \leq z_0$) for the saturation momentum. Note the slow dependence of the holographic saturation momentum on the longitudinal energy in the range $\ln(1/x) \leq 12$. Also note the nontrivial dependence on the impact parameter in the scattering amplitude or \mathbf{Q}_s , as opposed to a factorization approach done in most saturation and color glass-condensate models, compare [42] and references within.

VI. DIS IN CURVED SPACE

DIS of a lepton on a proton target can be viewed as a small size dipole scattering through a proton [2–8]. Dipole-dipole scattering using Wegner-Wilson loops to describe high-energy reactions of hadrons and photons was discussed in Refs. [43,44]. A holographic approach to DIS starting from the graviton limit and based on the critical string amplitude was elaborated in Refs. [39,40], see also Ref. [45]. Our approach is noncritical and rooted in the dipole-dipole formulation as detailed in Ref. [1] and briefly reviewed above.

The dipole-dipole cross section is useful for the determination of the inclusive proton structure function $F_2(x, Q^2)$ for small Bjorken x and large Q^2 . Specifically Refs. [7,8],

$$F_2(x, Q^2) = \frac{Q^2}{4\pi^2 \alpha_{EM}} (\sigma_T + \sigma_L), \quad (56)$$

and $\sigma_T + \sigma_L = \sigma_{\text{tot}}$ can be regarded as the total (virtual) photon-to-proton or dipole-to-dipole cross section. By the optical theorem

$$\sigma_{\text{tot}}(s) = -\frac{1}{s} \text{Im} \mathcal{T}(s, t=0), \quad (57)$$

whereby

$$\mathcal{T}(s, 0) = -2is \int d\mathbf{b}_\perp du du' \varphi_{\mathbf{P}}(u) \varphi_{\mathbf{T}}(u') (1 - e^{\mathbf{W}\mathbf{W}_{\text{poles}}}), \quad (58)$$

which is an averaging of the zz' -dipole-dipole cross section over the target $\varphi_{\mathbf{T}}(u')$ and projectile $\varphi_{\mathbf{P}}(u)$ dipole wave functions, respectively. Thus,

$$F_2(x, Q^2) = \frac{Q^2}{2\pi^2 \alpha_{EM}} \int d\mathbf{b}_\perp du du' \varphi_{\mathbf{P}}(u) \varphi_{\mathbf{T}}(u') \times (1 - e^{\mathbf{W}\mathbf{W}_{\text{poles}}}). \quad (59)$$

The integration in (58) and (59) involves all values of the impact parameter. While the validity of our approach following Ref. [1] is for large \mathbf{b} , we note that the dominant contribution to (58) and (59) stems from $\mathbf{b} \sim \sqrt{\alpha' \chi}$, which is large. Typically, the (target) proton and (projectile) photon dipole distributions are peaked, say

$$\varphi_{\mathbf{P}}(u) \equiv (\alpha_{EM}/\kappa^2) \delta(u - u_{\mathbf{P}}), \quad \varphi_{\mathbf{T}}(u') \equiv \delta(u - u_{\mathbf{T}}). \quad (60)$$

The normalization of the projectile (current) distribution in (60) is fixed empirically by the magnitude of the measured structure function F_2 . Of course, (60) are schematic wave functions that nonetheless capture the key physics and allow for analytical integration. We expect only small modifications if more realistic wave functions are used.

Inserting (60) into (59) and using the dipole-dipole cross section for $D_\perp = 3$ yields in the 1-pomeron exchange limit and in the conformal case

$$F_2(x, Q^2)|_{\text{conformal}} \approx \frac{g_s^2}{8\pi^2 \kappa^2} (2\pi\alpha')^{3/2} z_{\mathbf{T}} Q \frac{e^{(\alpha_{\mathbf{P}}-1)\chi}}{\sqrt{4\pi\mathbf{D}\chi}} \times (e^{-\frac{1}{4b_\perp} \ln^2(Qz_{\mathbf{T}})}) \quad (61)$$

and in the confining case

$$F_2(x, Q^2)|_{\text{confining}} \approx \frac{g_s^2}{8\pi^2 \kappa^2} (2\pi\alpha')^{3/2} z_{\mathbf{T}} Q \frac{e^{(\alpha_{\mathbf{P}}-1)\chi}}{\sqrt{4\pi\mathbf{D}\chi}} \times (e^{-\frac{1}{4b_\perp} \ln^2(Qz_{\mathbf{T}})} + e^{-\frac{1}{4b_\perp} \ln^2(Qz_0/z_{\mathbf{T}})}), \quad (62)$$

with $u_{\mathbf{P}} = \ln(z_0 Q)$, $u_{\mathbf{T}} = \ln(z_0/z_{\mathbf{T}})$. We have used the fact that

$$\begin{aligned} \mathbf{N}(T_\perp, u, u', t=0) \\ = \frac{e^{-T_\perp(M_0^2+1)}}{\sqrt{4\pi T_\perp}} (e^{-(u'-u)^2/4T_\perp} + e^{-(u'+u)^2/4T_\perp}) \end{aligned} \quad (63)$$

for $t = -\mathbf{q}_\perp^2 = 0$, after making use of the Fourier transform

$$\mathbf{N}(T_\perp, u, u', \mathbf{q}_\perp^2) = \int d\mathbf{b}_\perp e^{i\mathbf{q}_\perp \cdot \mathbf{b}_\perp} \mathbf{N}(T_\perp, u, u', \mathbf{b}_\perp). \quad (64)$$

Since the diffusion kernel in (63) is generic, the Q^2 dependency of the structure factor is sensitive to the \perp dimensions considered, $\mathbf{N} = \Delta/(zz')^{D_\perp-2}$.

The above approximation is justified when the photon momentum is sufficiently larger than the saturation scale, $Q \geq Q_s$, at all impact parameters \mathbf{b}_\perp . For the range of values for Q^2 , x considered to compare to the HERA data, the value for the proton structure function F_2 using the exponentiated 1-pomeron exchange (59) differs by less than 8% compared to F_2 from (62).

Figure 7 compares our result (62) to the HERA data [46], using the holographic parameter set quoted above. With our choice of parameters, our result for the 1-pomeron exchange amplitude in the confining background appears to fit the DIS data overall. Note that for $z_0 \sim z_{\mathbf{T}}$, the contribution from the hard wall is comparable to the conformal contribution. Thus, the conformal result (61) alone is not sufficient to describe the data with our set of parameters. Clearly our analysis is only qualitative, and a more thorough study of the parameter dependences and the fitting accuracy is needed.

Finally, we note that (47) defines the saturation line as a separatrix between the dilute and dense *wee-dipole* environment. For fixed virtuality Q^2 (inverse dipole size squared) and impact parameter \mathbf{b}_\perp , Fig. 8 shows the rapidities at which the cross section saturates in the black solid and dashed curves, i.e., when the condition in (47) is

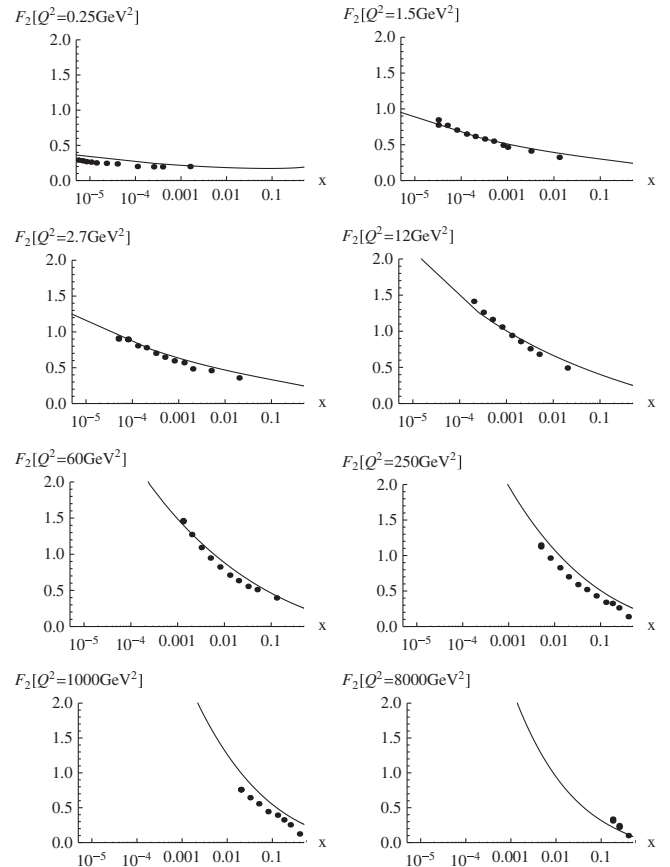


FIG. 7. Proton structure function F_2 in the confining background (62). See text.

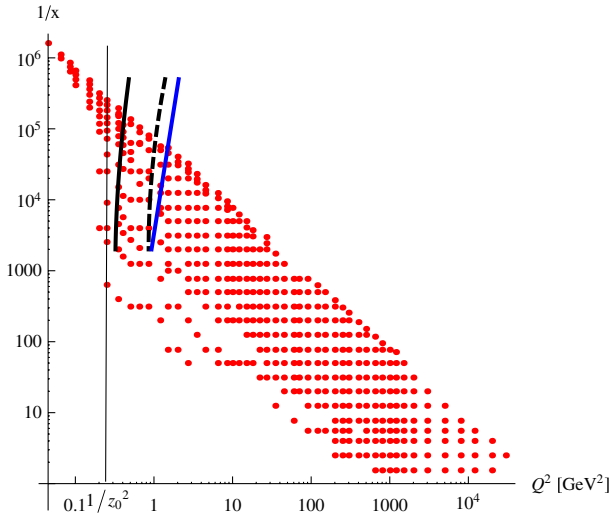


FIG. 8 (color online). Saturation lines in the confining background for $\mathbf{b}_\perp = 0 \text{ GeV}^{-1}$ (black, dashed curve) and $\mathbf{b}_\perp = 2 \text{ GeV}^{-1}$ (black, solid curve) in comparison to the Golec-Biernat Wuesthoff result (54) (blue, solid). The confining wall is at $1/z_0^2 = 1/4$. The dots are the measured HERA data. See text.

fulfilled. For comparison, the Golec-Biernat Wuesthoff result in (54) is shown as the blue solid curve. The points are the measured HERA data for the F_2 structure function. We note that (47) admits in general two distinct solutions for fixed x , Q^2 or χ , but only the one with the largest χ is shown which is warranted by our approximations. The HERA points at the left of the confining wall $1/z_0^2 = 1/4$ are well within the confining region. The confined holographic saturation lines are *stiff* in longitudinal energy as already noted in Fig. 5 above. For $b_\perp = 0$ the HERA points to the far right of the saturation line are well within the perturbative or dilute *wee-dipole* phase. Those close or to the left of the saturation line corresponds to the saturated *wee-dipole* phase. The closer they are to the confining wall $1/z_0^2 = 1/4$ the less perturbative they are in nature. The holographic saturation lines show that a large swath of the measured points at HERA which is well within the holographic saturation domain is sensitive to the impact parameter dependence \mathbf{b}_\perp of the saturation scale.

VII. CONCLUSIONS

Dipole-dipole scattering in holographic QCD is purely imaginary at large rapidity χ which is a key feature of QCD. It follows from the t -channel exchange of closed strings induced by a prompt longitudinal “electric” field. The pomeron with N -ality 1 is a closed string exchange triggered by a stringy Schwinger mechanism. The creation process fixes the pomeron slope, intercept, and weight (“residue”) in the elastic amplitude. From the open-closed string duality, Gribov’s diffusion follows from the presence of a large electric acceleration or Unruh temperature that causes the tachyonic mode of the dual open string to dimensionally reduce from D to D_\perp and diffuse.

In curved AdS space, the holographic direction is identified with the size of the dipole. The idea of Gribov diffusion appears as a tachyon diffusion in both virtuality and transverse space. In the conformal limit and for $D_\perp = 3$, the dipole-dipole scattering amplitude and its related *wee-dipole* density are found to be identical to the QCD results for onium-onium scattering using the QCD BFKL pomeron. The results are readily extended to confining AdS with a wall, and yield an explicit relation for the dipole saturation momentum as a function of rapidity χ [or equivalently $\ln(1/x)$] and impact parameter \mathbf{b}_\perp . For large impact parameter, the holographic saturation momentum is closely related to the GBW saturation momentum [13].

The dipole-dipole scattering amplitude in both conformal and confining AdS₃ is used to analyze the F_2 structure function. A comparison with DIS data from HERA shows that the x and Q^2 dependence of our holographic result are compatible with the data in the 1-pomeron exchange approximation, with no *a priori* need for an eikonal multi-pomeron resummation. This conclusion is only qualitative as a more thorough study of the parameter space of the holographic model as well as the fitting accuracy are needed.

ACKNOWLEDGMENTS

We would like to thank Gokce Basar and Ho-Ung Yee for discussions. This work was supported by the U.S. Department of Energy under Contract No. DE-FG-88ER40388.

-
- [1] G. Basar, D. E. Kharzeev, H.-U. Yee, and I. Zahed, *Phys. Rev. D* **85**, 105005 (2012).
 - [2] A. H. Mueller, *Nucl. Phys.* **B335**, 115 (1990).
 - [3] A. H. Mueller, *Nucl. Phys.* **B437**, 107 (1995).
 - [4] A. H. Mueller, *Nucl. Phys.* **B415**, 373 (1994).
 - [5] A. H. Mueller and B. Patel, *Nucl. Phys.* **B425**, 471 (1994).
 - [6] E. Iancu and A. H. Mueller, *Nucl. Phys.* **A730**, 460 (2004).
 - [7] N. N. Nikolaev and B. G. Zakharov, *Z. Phys. C* **49**, 607 (1991).
 - [8] N. Nikolaev and B. G. Zakharov, *Z. Phys. C* **53**, 331 (1992).
 - [9] G. P. Salam, *Nucl. Phys.* **B449**, 589 (1995).
 - [10] G. P. Salam, *Nucl. Phys.* **B461**, 512 (1996).
 - [11] H. Navelet, R. B. Peschanski, C. Royon, and S. Wallon, *Phys. Lett. B* **385**, 357 (1996).

- [12] H. Navelet and S. Wallon, *Nucl. Phys.* **B522**, 237 (1998).
- [13] K.J. Golec-Biernat and M. Wusthoff, *Phys. Rev. D* **59**, 014017 (1998).
- [14] E.A. Kuraev, L.N. Lipatov, and V.S. Fadin, *Sov. Phys. JETP* **45**, 199 (1978); Ya. Ya. Balitsky and L.N. Lipatov, *Sov. J. Nucl. Phys.* **28**, 822 (1978).
- [15] V.N. Gribov, in Proceedings of the 8th LNPI Winter School on Nuclear and Elementary Particle Physics, 1973 (unpublished), in *Gauge Theories and Quark Confinement* (Moscow, 2002), p. 3.
- [16] M. Rho, S.-J. Sin, and I. Zahed, *Phys. Lett. B* **466**, 199 (1999).
- [17] R.A. Janik and R.B. Peschanski, *Nucl. Phys.* **B565**, 193 (2000).
- [18] R.A. Janik and R.B. Peschanski, *Nucl. Phys.* **B625**, 279 (2002).
- [19] R.A. Janik and R.B. Peschanski, *Nucl. Phys.* **B586**, 163 (2000).
- [20] R.A. Janik, *Phys. Lett. B* **500**, 118 (2001).
- [21] J. Polchinski and M.J. Strassler, *Phys. Rev. Lett.* **88**, 031601 (2002).
- [22] J. Polchinski and M.J. Strassler, *J. High Energy Phys.* **05** (2003) 012.
- [23] R.C. Brower, J. Polchinski, M.J. Strassler, and C.I. Tan, *J. High Energy Phys.* **12** (2007) 005.
- [24] R.C. Brower, M.J. Strassler, and C.I. Tan, *J. High Energy Phys.* **03** (2009) 092.
- [25] L. Cornalba, M.S. Costa, and J. Penedones, *J. High Energy Phys.* **03** (2010) 133.
- [26] Y. Hatta, E. Iancu, and A.H. Mueller, *J. High Energy Phys.* **01** (2008) 063.
- [27] Y. Hatta, E. Iancu, and A.H. Mueller, *J. High Energy Phys.* **01** (2008) 026.
- [28] J.L. Albacete, Y.V. Kovchegov, and A. Taliotis, *J. High Energy Phys.* **07** (2008) 074.
- [29] J.L. Albacete, Y.V. Kovchegov, and A. Taliotis, *AIP Conf. Proc.* **1105**, 356 (2009).
- [30] L. Cornalba, M.S. Costa, and J. Penedones, *Phys. Rev. Lett.* **105**, 072003 (2010).
- [31] M. Luscher, *Nucl. Phys.* **B180**, 317 (1981).
- [32] O. Aharony and M. Field, *J. High Energy Phys.* **01** (2011) 065.
- [33] O. Nachtmann, *Ann. Phys. (N.Y.)* **209**, 436 (1991).
- [34] G. Veneziano, *Nucl. Phys.* **B117**, 519 (1976).
- [35] A.M. Polyakov, *Phys. Lett.* **103B**, 207 (1981).
- [36] D.E. Berenstein, R. Corrado, W. Fischler, and J.M. Maldacena, *Phys. Rev. D* **59**, 105023 (1999).
- [37] U.H. Danielsson, E. Keski-Vakkuri, and M. Kruczenski, *J. High Energy Phys.* **01** (1999) 002.
- [38] J.R. David, M.R. Gaberdiel, and R. Gopakumar, *J. High Energy Phys.* **04** (2010) 125.
- [39] R.C. Brower, M. Djuric, I. Sarcevic, and C.I. Tan, *J. High Energy Phys.* **11** (2010) 051.
- [40] R.C. Brower, M. Djuric, I. Sarcevic, and C.I. Tan, *arXiv:1106.5681*.
- [41] L.V. Gribov, E.M. Levin, and M.G. Ryskin, *Phys. Rep.* **100**, 1 (1983).
- [42] P. Tribedy and R. Venugopalan, *Nucl. Phys.* **A850**, 136 (2011); **A859**, 185(E) (2011).
- [43] O. Nachtmann, *arXiv:hep-ph/9609365*.
- [44] A.I. Shoshi, F.D. Steffen, and H.J. Pirner, *Nucl. Phys.* **A709**, 131 (2002).
- [45] Y.V. Kovchegov, Z. Lu, and A.H. Rezaeian, *Phys. Rev. D* **80**, 074023 (2009).
- [46] F.D. Aaron *et al.* (H1 and ZEUS Collaboration), *J. High Energy Phys.* **01** (2010) 109.